

Memory and universality in interface growth

Jacopo De Nardis,^{1,*} Pierre Le Doussal,^{2,†} and Kazumasa A. Takeuchi^{3,‡}

¹*Département de Physique, Ecole Normale Supérieure,*

PSL Research University, CNRS, 24 rue Lhomond, 75005 Paris, France

²*CNRS-LPTENS, Ecole Normale Supérieure, PSL Research University, 24 rue Lhomond, 75005 Paris, France.*

³*Department of Physics, Tokyo Institute of Technology,
2-12-1 Ookayama, Meguro-ku, Tokyo 152-8551, Japan.*

(Dated: May 26, 2022)

Understanding possible universal properties for systems far from equilibrium is much less developed than for their equilibrium counterparts and poses a major challenge to present day statistical physics. The study of aging properties, and how the memory of the past is conserved by the time evolution in presence of noise is a crucial facet of the problem. Recently, very robust universal properties were shown to arise in one-dimensional growth processes with local stochastic rules, leading to the Kardar-Parisi-Zhang universality class. Yet it has remained essentially unknown how fluctuations in these systems correlate at different times. Here we derive quantitative predictions for the universal form of the two-time aging dynamics of growing interfaces, which, moreover, turns out to exhibit a surprising breaking of ergodicity. We provide corroborating experimental observations on a turbulent liquid crystal system, which demonstrates universality. This may give insight into memory effects in a broader class of far-from-equilibrium systems.

Non-equilibrium dynamics is ubiquitous in nature, and takes diverse forms, such as avalanche motion in magnets and vortex lines¹⁻³, ultraslow relaxation in glasses⁴, unitary evolution towards thermalization in isolated quantum systems⁵, and flocking in living matter⁶. As a system tries to reach local equilibrium or stationarity, a great variety of behaviors can occur, such as aging dynamics and memory of past evolution. Finding general criteria and universal properties is therefore of fundamental importance.

Growth phenomena are prominent examples of non-equilibrium systems, which abound in physics⁷⁻¹⁰, biology^{7,11,12}, and beyond¹³. One important situation arises when a stable phase of a generic system expands into a non-stable (or meta-stable) one, in presence of noise. While spreading, the interface separating the two phases develops many non-trivial geometric and statistical features. A universal behavior then emerges, unifying many growing phenomena into a few universality classes, irrespective of their microscopic details. The most generic one, for local growth rules, is the celebrated Kardar-Parisi-Zhang (KPZ) class, now substantiated by many experimental examples, such as growing turbulence of liquid crystal^{8,9}, propagating chemical fronts¹³, paper combustion¹⁰ and bacteria colony growth¹¹. For one-dimensional interfaces growing in a plane, as studied in many experiments, it is characterized by the following KPZ equation¹⁴:

$$\partial_t h(x, t) = \nu \partial_x^2 h(x, t) + \frac{\lambda_0}{2} (\partial_x h(x, t))^2 + \sqrt{D} \xi(x, t) \quad (1)$$

describing the motion of an interface of height $h(x, t)$ at point $x \in \mathbb{R}$ at time t , driven by a unit space-time white noise $\xi(x, t)$. Recently, this problem became an outstanding example where a wealth of universal statistical properties can be solved exactly, from the KPZ equation and related lattice models¹⁵⁻²². At

large time, the height evolves as $h(0, t) = v_\infty t + (\Gamma t)^{1/3} \tilde{h}_t$ with system-dependent parameters v_∞, Γ and a stochastic variable \tilde{h}_t that carries universal information of the fluctuations. Remarkably, in the limit $t \rightarrow \infty$, \tilde{h}_t follows one of a few non-Gaussian universal distributions, selected only by the global geometric shape of the initial condition $h(x, t = 0)$: in particular, the GUE Tracy-Widom distribution²³, $F_2(\sigma)$, when $h(x, 0)$ is narrowly curved (droplet initial condition¹⁷⁻²⁰, see Fig. 1A) and its GOE variant, $F_1(\sigma)$, when $h(x, 0)$ is a flat surface²¹. These two distributions also describe the fluctuations of the largest eigenvalue of a gaussian random matrix drawn from the unitary (GUE) or orthogonal (GOE) ensembles, revealing a striking connection to the theory of random matrices^{16,24}. An additional universal distribution, the Baik-Rains distribution¹⁵, characterizes the stationary state of the growth and can be reached²² by choosing $h(x, 0)$ as Brownian motion in x .

This geometry-dependent universality was tested and confirmed experimentally, in studies on growing interfaces of liquid-crystal turbulence^{8,9}. The experiments also allowed to investigate time-correlation properties that were inaccessible by analytical approaches. This revealed an anomalous memory effect for the droplet case⁹, where fluctuations in h keep indefinite memory of the past, in contrast to the naive expectation that memory is eventually lost. This persistence of memory, signaling ergodicity breaking in the time evolution of the droplet case, is quantified by the covariance $C(t_1, t_2) = \text{cov}[h(0, t_1), h(0, t_2)]$, which remains strictly positive in the limit $t_2/t_1 \rightarrow \infty$ ^{9,25}. Theoretically, however, such two-time quantities remain analytically intractable, except for a few exceptional results^{26,27} that however are too involved to produce practical predictions.

Here we show the first analytical result for the joint probability density function (JPDF) of the height h at two different times, t_1 and $t_2 = (1 + \Delta)t_1$, with the

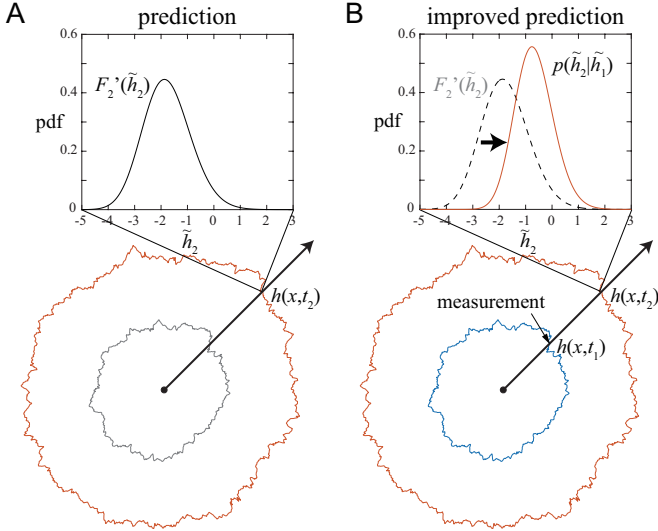


FIG. 1: Concept of the two-time joint probability density function (JPDF). (A) If we only measure the height at time t_2 , we can only predict that a fluctuation of the height $h(x, t_2)$ will be drawn (asymptotically) from the GUE Tracy-Widom distribution, $F_2'(\tilde{h}_2)$, with the rescaled height $\tilde{h}_2 := \tilde{h}_{t_2} = \frac{h(x, t_2) - v_\infty t_2}{(\Gamma t_2)^{1/3}}$. (B) In contrast, using the past information at time t_1 , $\tilde{h}_1 := \tilde{h}_{t_1} = \frac{h(x, t_1) - v_\infty t_1}{(\Gamma t_1)^{1/3}}$, we can make a more precise prediction about \tilde{h}_2 . Instead of $F_2'(\tilde{h}_2)$ (dashed line), the prediction is now given by the conditional probability density $p(\tilde{h}_2|\tilde{h}_1)$ (red line; curve for $\tilde{h}_1 = 0$ is shown), which is directly obtained from the JPDF $P_\Delta(\sigma_1, \sigma)$ (2) we provide here: $p(\tilde{h}_2|\tilde{h}_1) \propto P_\Delta(\tilde{h}_1, \frac{(1+\Delta)^{1/3}\tilde{h}_2 - \tilde{h}_1}{\Delta^{1/3}})$ with normalization $\int p(\tilde{h}_2|\tilde{h}_1)d\tilde{h}_2 = 1$. Note that the sharper distribution (red) indicates that the prediction is more accurate, and the expected value of \tilde{h}_2 is shifted due to the memory effect from time t_1 .

droplet initial condition. It is valid in a wide range of parameters and agrees remarkably well with experimental and numerical data (see below). We focus on the limit $t_1, t_2 \rightarrow \infty$ with their ratio $t_2/t_1 = 1 + \Delta$ kept finite, so that the obtained correlations are expected to be universal within the KPZ class. More precisely, we compute the JPDF for the rescaled height $\tilde{h}_1 := \tilde{h}_{t_1} = \frac{h(0, t_1) - v_\infty t_1}{(\Gamma t_1)^{1/3}}$ and the rescaled two-time height difference $\tilde{h}_{12} := \frac{h(0, t_2) - h(0, t_1) - v_\infty t_1 \Delta}{(\Gamma t_1 \Delta)^{1/3}}$. It is defined as

$$P_\Delta(\sigma_1, \sigma) d\sigma_1 d\sigma = \lim_{t_1 \rightarrow \infty} \text{Prob} \left(\sigma_1 \leq \tilde{h}_1 \leq \sigma_1 + d\sigma_1, \sigma \leq \tilde{h}_{12} \leq \sigma + d\sigma \right). \quad (2)$$

and quantifies how much memory of the configuration at the earlier time t_1 is retained at the later time t_2 , as illustrated in Fig. 1B. It allows to calculate the conditional cumulants $\langle \tilde{h}_{12}^n \rangle_{\tilde{h}_1 > \sigma_{1c}}^c$, i.e., the cumulants of the variable \tilde{h}_{12} conditioned to realizations with \tilde{h}_1 larger than some fixed value σ_{1c} . It also allows to predict the rescaled

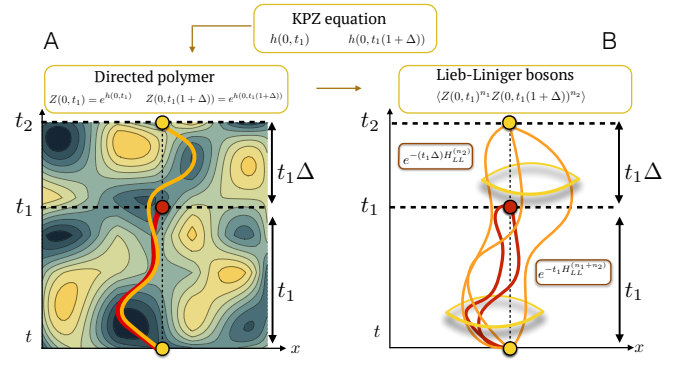


FIG. 2: Representation of the KPZ height with directed polymers and mapping to quantum mechanics. (A) From (1) $Z(x, t) = e^{h(x, t)}$ satisfies a linear stochastic equation, thus is given by a sum over space-time paths, interpreted as the canonical partition sum of a directed polymer (DP) with endpoints $(0, 0)$ and (x, t) in a random potential (shown as contour plot) equal to $-\xi(x, t)$. The function $P_\Delta(\sigma_1, \sigma)$ maps to the JPDF of the free energies of two DP starting both in $(0, 0)$ but ending in $(0, t_1)$ and $(0, t_2 = t_1(1 + \Delta))$: shown is a typical configuration of these 2 paths, which tend to visit the lower valleys of the potential (bluer regions), i.e. faster growth regions, compatible with their boundary conditions and kinetic energies, which tends to minimize their length. The two paths tend to overlap in the time interval $[0, t_1]$, accounting for ergodicity breaking (see text). (B) The JPDF (2) is obtained (Methods) from the joint integer moments $\langle Z(0, t_1)^{n_1} Z(0, t_2)^{n_2} \rangle$, averaged over realizations of the random potential. They are given by the quantum mechanical amplitude of the following process: $n_1 + n_2$ bosons with pair-wise attractive potential (represented by the red belt) evolve from $x = 0$ in imaginary time with the Lieb-Liniger Hamiltonian up to time t_1 . At time $t = t_1$, n_1 of them are annihilated at $x = 0$, while the other n_2 keep evolving up to time $t = t_1(1 + \Delta)$ where they are all finally destroyed in $x = 0$ (see (7) in Methods).

covariance under the same conditioning, defined as

$$C_{\Delta, \sigma_{1c}} = \frac{C(t_1, t_2)_{\tilde{h}_1 > \sigma_{1c}}}{C(t_1, t_1)_{\tilde{h}_1 > \sigma_{1c}}} = 1 + \Delta^{1/3} \frac{\text{cov}[\tilde{h}_1, \tilde{h}_{12}]_{\tilde{h}_1 > \sigma_{1c}}}{\langle \tilde{h}_1^2 \rangle_{\tilde{h}_1 > \sigma_{1c}}^c}. \quad (3)$$

These quantities, computed here analytically for the first time, allow to probe memory effects and quantify the breaking of ergodicity in the dynamics.

To derive a numerically tractable expression for the JPDF (2), we exploit the fact that the KPZ equation is equivalent to a (statistical mechanics) problem of space-time paths (i.e. “growth histories”) in a random potential, which is further mapped into a quantum problem of bosons (see Fig. 2). Their Hamiltonian is the Lieb-Liniger Hamiltonian with attractive interaction, extensively studied recently in the context of integrable out-of-equilibrium dynamics²⁸. Integrability of this dual quantum model allows us to derive an analytical expression for $P_\Delta(\sigma_1, \sigma)$, in the form $P_\Delta(\sigma_1, \sigma) = P_\Delta^{(1)}(\sigma_1, \sigma)(1 + \mathcal{O}(e^{-\frac{4}{3}\sigma_1^{3/2}}))$ with $P_\Delta^{(1)}(\sigma_1, \sigma)$ exactly determined in this

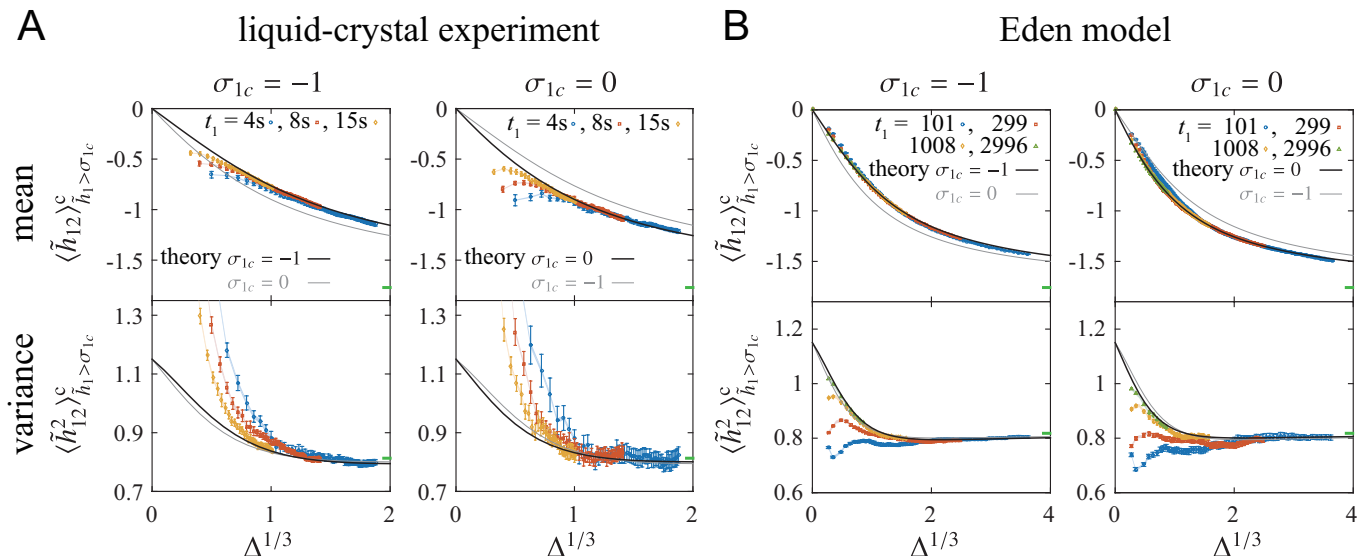


FIG. 3: Test of the theoretical prediction for the conditional mean $\langle \tilde{h}_{12} \rangle_{\tilde{h}_1 > \sigma_{1c}}^{\xi}$ and variance $\langle \tilde{h}_{12}^2 \rangle_{\tilde{h}_1 > \sigma_{1c}}^{\xi}$ with the liquid-crystal experiment (A) and the Eden-model simulation (B). Here the results for $\sigma_{1c} = -1$ and 0 are shown (see also Fig. S3 for $\sigma_{1c} = -1.5$). Data at different t_1 are shown in different colors and symbols. The regions of overlapped data indicate the asymptotic Δ -dependence, which is found to be in excellent agreement with the theoretical predictions (black lines), without any fitting parameter. For comparison, the theoretical curves with another value of σ_{1c} are shown by gray thin lines. The error bars indicate the standard errors, and the shaded areas show the uncertainty due to the estimation error in v_{∞} and Γ . To reduce the effect of finite-time corrections, here we used such realizations that satisfy $\tilde{h}_1 > \tilde{h}_{1c}$ with $\text{Prob}[\tilde{h}_1 \geq \tilde{h}_{1c}] = 1 - F_2(\sigma_{1c})$. The deviation of the non-overlapped data is due to finite-time corrections, which decay as t_1^{-1} , see Fig. S4). Note that the asymptotic theoretical curves converge to the Baik-Rains values (mean 0, variance 1.1504) at $\Delta \rightarrow 0$ and the GUE Tracy-Widom values (mean -1.7711, variance 0.8132, indicated in the figures by the green bars) at $\Delta \rightarrow \infty$.

work. It is written (see Methods) as a trace of kernels acting on $\mathbb{R} \times \mathbb{R}$:

$$P_{\Delta}^{(1)}(\sigma_1, \sigma) = \left(\partial_{\sigma_1} \partial_{\sigma} - \Delta^{-1/3} \partial_{\sigma}^2 \right) \times \left\{ F_2(\sigma) \text{Tr} \left[\Delta^{1/3} \Pi_{\sigma} K_{\sigma_1}^{\Delta} \Pi_{\sigma} (I - \Pi_{\sigma} K_{\text{Ai}} \Pi_{\sigma})^{-1} - \Pi_{\sigma_1} K_{\text{Ai}} \right] \right\}. \quad (4)$$

where Π_{σ} projects on the interval $[\sigma, +\infty) \in \mathbb{R}$, I is the identity operator and ∂_{σ} denotes partial derivatives. The expression involves the well-known Airy kernel $K_{\text{Ai}}(r, r')$ from random matrix theory²³ and a novel kernel $K_{\sigma_1}^{\Delta}(r, r')$ described in Methods.

The formula (4) is simple enough for numerical evaluations (see Methods) for any value of σ_1 inside its expected validity range (specifically $\sigma_1 \gtrsim -1.5$; see SI, Sec. B). This allows us to perform direct tests of the theoretical predictions, both experimentally and numerically, without any fitting parameters. Experimentally, we study growing interfaces of liquid-crystal turbulence, which were previously shown to be in the KPZ class^{8,9}. Measuring the conditional cumulants $\langle \tilde{h}_{12}^n \rangle_{\tilde{h}_1 > \sigma_{1c}}^{\xi}$ and extracting their asymptotic forms, indicated by overlapping of data sets with different t_1 , we find an excellent agreement with the theoretical predictions (Figs. 3A and S3A). The same quality of agreement is also obtained with numerical simulations of the off-lattice Eden model²⁹ (Figs. 3B and S3B). We also measure the con-

ditional covariance (3) and find agreement both experimentally and numerically (Fig. 4). This indicates that our predictions describe universal time correlation of the droplet KPZ interfaces.

Moreover, our theory shows analytically for the first time the crossover between different probability distributions for \tilde{h}_{12} , as Δ varies (see Fig. 5). In the limit of close times, $t_2/t_1 \rightarrow 1^+$ the JPDF (4) factorizes and $\tilde{h}_1, \tilde{h}_{12}$ become two independent random variables following respectively the GUE Tracy-Widom and Baik-Rains distributions. The emergence of the Baik-Rains distribution is direct evidence of the approach to the KPZ stationary state when $t_2/t_1 \rightarrow 1^{+25}$. As time separation increases a non-trivial aging form develops and for $\Delta \rightarrow \infty$ the joint statistics factorizes into the product of two GUE Tracy-Widom distributions. The next order correction, of order $\mathcal{O}(\Delta^{-1/3})$, gives access to the asymptotic value of the persistent correlation $C_{\Delta \rightarrow \infty, \sigma_{1c}}$: as σ_{1c} decreases from $+\infty$ to $-\infty$, i.e., the unconditioned case, it is predicted to decrease from 1 to a strictly positive value estimated to be ≈ 0.6 (see SI, Sec. C), which is consistent with our numerical data (Fig. 4C, purple stars). The directed polymer/growth-history path representation enlightens this ergodicity breaking phenomenon. As shown in Fig. 2, the two polymers tend to visit the same minima of the random potential, thus sharing a finite fraction of their paths (growth histories) in the time interval $[0, t_1]$.

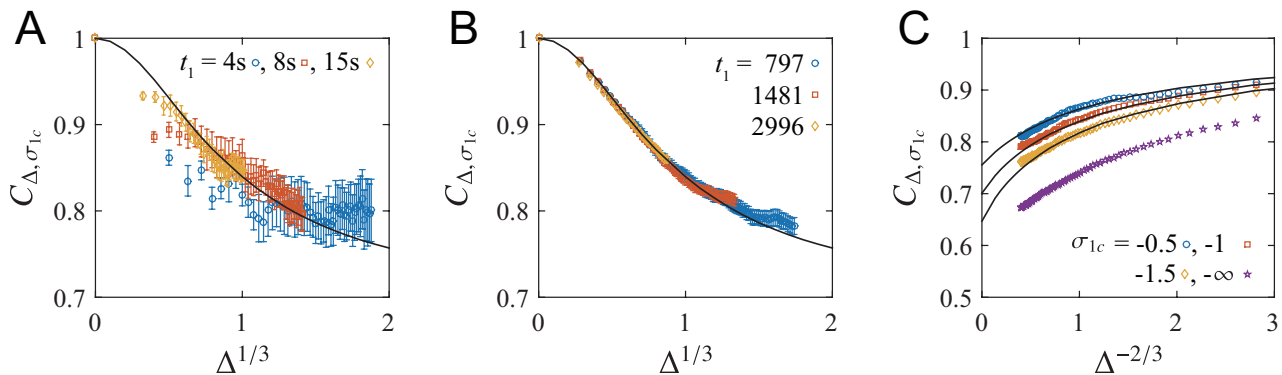


FIG. 4: The conditional covariance $C_{\Delta, \sigma_{1c}} = C(t_1, t_2)_{\tilde{h}_1 > \sigma_{1c}} / C(t_1, t_1)_{\tilde{h}_1 > \sigma_{1c}}$ ((3)). **a, b**, Experimental (A) and numerical (B) results for $\sigma_{1c} = -1$ and with varying t_1 (symbols), compared with the theoretical prediction (black line). The error bars indicate the standard errors. To reduce the effect of finite-time corrections, here we used such realizations that satisfy $\tilde{h}_1 > \tilde{h}_{1c}$ with $\text{Prob}[\tilde{h}_1 \geq \tilde{h}_{1c}] = 1 - F_2(\sigma_{1c})$. **c**, Numerical data for $t_1 = 1008$ and for $\sigma_{1c} = -0.5, -1, -1.5$ and $-\infty$ (unconditioned). Error bars are omitted here for the sake of visibility. The black lines indicate the theoretical predictions for finite σ_{1c} . At large Δ and for any σ_{1c} they converge to their asymptotic values as $C_{\Delta \rightarrow \infty, \sigma_{1c}} + A_{\sigma_{1c}} \Delta^{-2/3} + B_{\sigma_{1c}} \Delta^{-1} + \dots$. For $\sigma_{1c} = -\infty$ (the unconditioned case), the theory suggests a strictly positive asymptotic value, specifically $C_{\infty, -\infty} \approx 0.6$, which is consistent with the trend of the unconditioned data set in the panel **c** (purple stars).

This translates into a finite correlation even in the limit $t_2 \gg t_1$, which our theory quantifies: as σ_{1c} is increased, noise realizations with faster growth are selected, and this fraction approaches unity: memory becomes perfect, and $C_{\Delta \rightarrow \infty, \sigma_{1c}} \rightarrow 1$. This is consistent with the experimental and numerical observation (Fig. 4).

This universality in multi-time correlations, accompanied with ergodicity breaking could be explored in a broader class of growth problems both within and beyond the KPZ class³⁰. In expanding geometries, we expect similar persistence of memory when the spatial scale of dynamical correlations, $x \sim t_1^\zeta$ ($\zeta = 2/3$ for KPZ) grows slower than the expanding substrate radius (here $\sim t_1$). It should also be relevant for other non-equilibrium systems, such as driven Bose-Einstein condensates³¹ and genetic segregation in expanding bacterial colonies¹², both shown to relate to KPZ.

We thank P. Calabrese, I. Corwin, and K. Johansson for discussions. This work is supported in part by KAKENHI from JSPS, Nos. JP25103004, 16H04033, 16K13846 (K.A.T.), LabEX ENS-ICFP:ANR-10-LABX-0010/ANR-10-IDEX-0001-02 PSL* (J.D.N.), and the National Science Foundation under Grant No. NSF PHY11-25915.

METHODS

The KPZ equation and the two-time JPDP via the directed polymer

In the theory part of this work (including the caption of Fig. 2) we use everywhere the scales $x^* = \frac{(2\nu)^3}{D\lambda_0^2}$, $t^* = \frac{2(2\nu)^5}{D^2\lambda_0^4}$, $h^* = \frac{2\nu}{\lambda_0}$ as units of space, time and height,

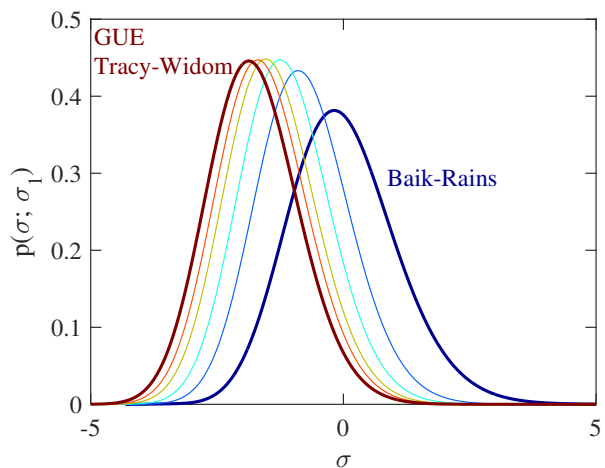


FIG. 5: Predicted crossover from the Baik-Rains distribution ($\Delta \rightarrow 0$, i.e. $t_2/t_1 \rightarrow 1^+$) to the GUE Tracy-Widom distribution ($\Delta \rightarrow \infty$, i.e. $t_2/t_1 \rightarrow \infty$), for the conditional probability of the rescaled height difference \tilde{h}_{12} , $p(\sigma|\sigma_1)d\sigma = \text{Prob}(\sigma < \tilde{h}_{12} < \sigma + d\sigma | \tilde{h}_1 = \sigma_1) \propto P_\Delta(\sigma_1, \sigma)$. Plotted here is $p(\sigma|\sigma_1) \propto P_\Delta^{(1)}(\sigma_1, \sigma)$ predicted from (4), for $\sigma_1 = 0$ and for $\Delta^{1/3} = 0, 0.7, 1.4, 2.8, 5.6, \infty$ from right to left.

respectively. In other words, $x/x^*, t/t^*, h/h^*$ are simply denoted by x, t, h , respectively. This amounts to setting $\nu = 1$, $\lambda_0 = 2$ and $D = 2$ in the KPZ equation (1), which leads to $\Gamma = 1$.

To solve the KPZ equation, we use the Cole-Hopf mapping³², which, given an initial condition $h(x, 0)$, allows to write the height at time t as $e^{h(x,t)} = Z(x, t) \equiv \int dy Z(x, t|y, 0) e^{h(y,0)}$. Here $Z(x, t|y, 0)$ is the partition function of a continuum elastic polymer parametrized by

the function $x(\tau)$ with $\tau \in [0, t]$ (its elastic energy given by $\frac{1}{4}(\frac{dx(\tau)}{d\tau})^2$) in the random potential $-\sqrt{2}\eta(x, t)$ with fixed endpoints at (x, t) and $(y, 0)$:

$$Z(x, t|y, 0) = \int_{x(0)=y}^{x(t)=x} Dx e^{-\int_0^t d\tau [\frac{1}{4}(\frac{dx}{d\tau})^2 - \sqrt{2}\eta(x(\tau), \tau)]} \quad (5)$$

We focus on the droplet initial condition $h_{w_0}(x, 0) = -w_0|x|$ in the limit $w_0 \rightarrow +\infty$. Since $h(x, t) = \ln Z(x, t|0, 0)$, the droplet height profile $h(x, t)$ corresponds to the (minus) free energy of a DP (at unit temperature) in a random potential, going from the point $(0, 0)$ to (x, t) .

To obtain the JPDF we introduce the generating function

$$g_{\Delta, t_1}(\sigma_1, \sigma) = \left\langle \exp \left(e^{-t_1^{1/3}(\tilde{h}_{t_1} - \sigma_1) - t_2^{1/3}(\tilde{h}_{t_2} - (\sigma_1 + \Delta^{1/3}\sigma))} \right) \right\rangle \quad (6)$$

In the limit $t_1, t_2 \rightarrow +\infty$ it becomes equal to $g_{\Delta}(\sigma_1, \sigma)$, the cumulative JPDF of $\tilde{h}_{t_1}, \tilde{h}_{t_2}$. Hence it yields the desired JPDF (2) as $P_{\Delta}(\sigma_1, \sigma) = (\partial_{\sigma_1} \partial_{\sigma} - \Delta^{-1/3} \partial_{\sigma}^2) g_{\Delta}(\sigma_1, \sigma)$. On the other hand the first exponential in (6) can be expanded as a series in positive integer powers of $e^{t_1^{1/3}\tilde{h}_{t_1}} = Z(0, t_1)$ and $e^{t_2^{1/3}\tilde{h}_{t_2}} = Z(0, t_2)$. The necessary ingredients are then the joint moments $\langle Z(0, t_1)^{n_1} Z(0, t_2)^{n_2} \rangle$. After integration over the Gaussian white noise η , using replica techniques introduced by Kardar³², they can be expressed in terms of quantum mechanical amplitudes for a problem of attractive bosons in one dimension

$$\langle Z(0, t_1)^{n_1} Z(0, t_2)^{n_2} \rangle = \prod_{j=1}^{n_2} \int_{-\infty}^{\infty} dy_j \quad (7)$$

$$\times \langle \vec{0}_{n_2} | e^{-(t_1 \Delta) H_{LL}^{(n_2)}} | \vec{y}_{n_2} \rangle \langle \vec{y}_{n_2}, \vec{0}_{n_1} | e^{-t_1 H_{LL}^{(n_2+n_1)}} | \vec{0}_{n_2}, \vec{0}_{n_1} \rangle$$

where $|\vec{y}_{n_2}, \vec{x}_{n_1}\rangle$ denotes the quantum state where n_2 bosons are in positions $\vec{y} = \{y_j\}_{j=1}^{n_2}$ and n_1 bosons are in positions $\vec{x} = \{x_j\}_{j=1}^{n_1}$ (see Fig. 2). Here H_{LL}^n is the Lieb-Liniger Hamiltonian for n attractive bosons interacting with a point-wise potential

$$H_{LL}^{(n)} = - \sum_{j=1}^n \partial_{x_j}^2 - 2 \sum_{i<j}^n \delta(x_i - x_j) - \frac{n}{12} \quad (8)$$

The Hamiltonian (1) is integrable and all its eigenstates with n particles, $|\mu_n\rangle$, and eigenvalues, E_{μ_n} , are explicitly known. We then expand (7) on the complete basis inserting $1 = \sum_{\mu_n} |\mu_n\rangle \langle \mu_n|$ in each factor. This leads to an expression for each joint moment. The full summation over all eigenstates and n_1, n_2 is beyond reach at present, but we are able to find an analytical expression for a partial summation when the second factor in (7) is restricted to the ground state (see SI, Sec. A). This already contains important information, since it leads to $g_{\Delta}^{(1)}(\sigma_1, \sigma)$, equal to $g_{\Delta}(\sigma_1, \sigma)$ up to super-exponentially

small corrections when σ_1 is positive. Finally we then obtain the JPDF (4) with the Kernel $K_{\sigma_1}^{\Delta}$:

$$K_{\sigma_1}^{\Delta}(r, r') = \int_0^{\infty} dz_1 dz_2 \text{Ai}(-z_1 + r) \text{Ai}(-z_2 + r') \times K_{\text{Ai}}(z_1 \Delta^{1/3} + \sigma_1, z_2 \Delta^{1/3} + \sigma_1) \quad (9)$$

where $K_{\text{Ai}}(r, r') = \int_0^{\infty} dz \text{Ai}(r+z) \text{Ai}(r'+z)$ is the Airy kernel.

Numerical evaluations

For the numerical evaluation of (4) and of the Tracy-Widom and Baik-Rains distributions ($F_2(\sigma)$ and $F_0(\sigma)$), we use a Gaussian quadrature discretization method to transform the continuous kernels into discrete square matrices. This amounts to approximate an integral with its discrete sum $\int_s^{\infty} dx f(x) \rightarrow \sum_{j=1}^n f(x_j) w_j$ where $\{x_i\}_{i=1}^n$ are the n quadrature points $x_j \in [s, +\infty]$ and $\{w_i\}_{i=1}^n$ the corresponding weights. Traces and Fredholm determinants become standard traces and determinants of square matrices

$$\text{Tr}[\Pi_s K] \rightarrow \text{Tr}_{i,j=1}^n [K(x_i, x_j) w_i] \quad (10)$$

$$\det[1 - \Pi_s K] \rightarrow \det_{i,j=1}^n [\delta_{i,j} - w_j K(x_i, x_j)] \quad (11)$$

and the inverse of the kernel $(I - \Pi_s K_{\text{Ai}} \Pi_s)^{-1}$ is evaluated as the simple inverse of the corresponding discretized matrix. The number n depends on the particular quadrature rule and on the kernel but in general we find good convergence for $n \sim 50$ with a standard Gaussian quadrature rule (for the numerical evaluation of $F_2(\sigma) = \text{Det}[I - \Pi_{\sigma} K_{\text{Ai}}]$ exponential fast convergence with n was proved in³³).

Liquid crystal experiment

For the experiment, we studied growing interfaces in electrically driven turbulence of nematic liquid crystal, which were previously shown to be in the KPZ class^{8,9}. The interfaces constitute boundaries between two distinct turbulent states, called the dynamic scattering modes (DSM) 1 and 2 in the literature, which are characterized by the absence and abundance, respectively, of sustained topological defects in the director field. Under the experimental condition used here, DSM2 is stable while DSM1 is only metastable. Therefore, by nucleating DSM2 locally amid DSM1, using ultraviolet laser pulses as a trigger, one can observe a growing cluster of DSM2, bordered by a fluctuating circular interface. We generated 955 such circular interfaces, for which the non-universal parameters v_{∞} and Γ were previously determined with high precision⁹. See Ref.⁹ for more detailed descriptions of the experimental system.

Eden numerics

The numerical test was carried out with an off-lattice version of the Eden model, which was introduced in Ref.²⁹ as a convenient model to study circular interfaces with isotropic growth speed. The model consists of a cluster of round particles of unit diameter, added one by one, starting from a single particle placed in two-dimensional space. At each time step, one attempts to add a new particle, next to a randomly chosen particle in a randomly chosen direction. The attempt is adopted if

it does not overlap with any existing particle, otherwise the attempt is simply withdrawn. In either case, time is increased by $1/N$, where N denotes the number of particles. A circular interface is then obtained as the outmost perimeter of the cluster. Here we generated 5000 independent realizations of such circular interfaces, using an efficient algorithm described in Ref.²⁹. The height function $h(x, t)$ is defined as in the experiment. The values of v_∞ and Γ were taken from those from an extensive numerical study reported in Ref.³⁴.

-
- * jacopo.de.nardis@phys.ens.fr
† ledou@lpt.ens.fr
‡ kat@kaztake.org
- ¹ Xu, D., Guohong, L., Andrei, E. Y., Greenblatt, M. and Shuk, P. Ageing memory and glassiness of a driven vortex system. *Nature Phys.* **3**, 111-114 (2007).
 - ² Papanikolaou, S. , Bohn, F., Sommer, R. L., Durin, G. , Zapperi, S., Sethna, J. P. Universality beyond power laws and the average avalanche shape. *Nature Physics* **7**, 316-320 (2011).
 - ³ Hwa, T. From vortices to genomics, *Nature* **399**, 17-18 (1999).
 - ⁴ Kurchan, J. In and out of equilibrium. *Nature* **433**, 222-225 (2005).
 - ⁵ Eisert, J. , Friesdorf, M. and Gogolin, C. Quantum many-body systems out of equilibrium. *Nature Phys.* **11**, 124-130 (2015).
 - ⁶ Chen, L., Lee, C. F., Toner, J. Surprising mappings of 2D polar active fluids to 2D soap and 1D sandblasting. *Nature Communications* **7**, 12215 (2016).
 - ⁷ Barabasi, A.-L., Stanley, H.E. Fractal concepts in surface growth, *Cambridge University Press* (1995).
 - ⁸ Takeuchi, K. A. and Sano, M. Universal Fluctuations of Growing Interfaces: Evidence in Turbulent Liquid Crystals. *Phys. Rev. Lett.* **104**, 230601 (2010).
 - ⁹ Takeuchi, K. A. and Sano, M. Evidence for Geometry-Dependent Universal Fluctuations of the Kardar-Parisi-Zhang Interfaces in Liquid-Crystal Turbulence. *J. Stat. Phys.* **147**, 853–890 (2012).
 - ¹⁰ Maunuksela, J., Myllys, M., Kähkönen, O.-P., Timonen, J., Provatas, N., Alava, M. J. and Ala-Nissila, T. Kinetic Roughening in Slow Combustion of Paper. *Phys. Rev. Lett.* **79**, 1515–1518 (1997).
 - ¹¹ Wakita, J.-i., Itoh, H., Matsuyama, T. and Matsushita, M. Self-Affinity for the Growing Interface of Bacterial Colonies. *J. Phys. Soc. Jpn.* **66**, 67-72 (1997).
 - ¹² Hallatschek, O., Hersen, P., Ramanathan, S. Nelson, D. R. Genetic drift at expanding frontiers promotes gene segregation. *Proc. Natl Acad. Sci.* **104**, 19926-19930 (2007).
 - ¹³ Atis, S., Dubey, A. K., Salin, D., Talon, L., Le Doussal, P. and Wiese, K. J. Experimental Evidence for Three Universality Classes for Reaction Fronts in Disordered Flows. *Phys. Rev. Lett.* **114**, 234502 (2015).
 - ¹⁴ Kardar M., Parisi G. and Zhang Y.C. Dynamical scaling of growing interfaces. *Phys. Rev. Lett.* **56**, 889 (1986).
 - ¹⁵ Baik, J. and Rains, E.M. Limiting distributions for a polynuclear growth model with external sources, *J. Stat. Phys.* **100**, 523 (2000)
 - ¹⁶ Prahofer, M. and Spohn, H. Universal distributions for growth processes in 1+1 dimensions and random matrices. *Phys. Rev. Lett.* **84**, 4882 (2000).
 - ¹⁷ Sasamoto, T. and Spohn, H. One-Dimensional Kardar-Parisi-Zhang Equation: An Exact Solution and its Universality. *Phys. Rev. Lett.* **104**, 230602 (2010)
 - ¹⁸ Calabrese, P., Le Doussal, P. and Rosso, A. Free-energy distribution of the directed polymer at high temperature. *EPL* **90**, 20002 (2010)
 - ¹⁹ Dotsenko, V. Bethe ansatz derivation of the Tracy-Widom distribution. *EPL* **90**, 20003 (2010).
 - ²⁰ Amir, G., Corwin, I., Quastel, J. Probability distribution of the free energy of the continuum directed random polymer in 1+ 1 dimensions. *Comm. Pure Appl. Math* **64**, 466 (2011)
 - ²¹ Le Doussal, P. and Calabrese, P. Exact Solution for the Kardar-Parisi-Zhang Equation with Flat Initial Conditions. *Phys. Rev. Lett.* **106**, 250603 (2011).
 - ²² Imamura, T. and Sasamoto, T. Exact Solution for the Stationary Kardar-Parisi-Zhang Equation. *Phys. Rev. Lett.* **108**, 190603 (2012).
 - ²³ Tracy, C.A. and Widom, H. Level-spacing distributions and the Airy kernel. *Comm. Math. Phys.* **159**, 151 (1994)
 - ²⁴ Kriecherbauer, T. and Krug, J. A pedestrians view on interacting particle systems, KPZ universality and random matrices. *J. Phys. A: Math. Theor.* **43**, 403001 (2010).
 - ²⁵ Ferrari, P. L. and Spohn, H. On time correlations for KPZ growth in one dimension. *SIGMA* **12**, 074 (2016).
 - ²⁶ Dotsenko, V. Two-time free energy distribution function in (1+1) directed polymers. *J. Stat. Mech* P06017 (2013)
 - ²⁷ Johansson, K. Two-time distribution in Brownian directed percolation. *Commun. Math. Phys.* 1-52 (2016)
 - ²⁸ Calabrese, P. and Caux, J.-S. Correlation functions of the one-dimensional attractive Bose gas. *Phys. Rev. Lett.* **98**, 150403 (2007)
 - ²⁹ Takeuchi, K. A. Statistics of circular interface fluctuations in an off-lattice Eden model. *J. Stat. Mech.* P05007 (2012).
 - ³⁰ Carrasco, I. S. S., Oliveira, T. J. Universality and geometry dependence in the class of the nonlinear molecular beam epitaxy equation. arXiv:1606.06097.
 - ³¹ He, L., Sieberer, L. M., Altman, E., Diehl, S. Scaling properties of one-dimensional driven-dissipative condensates. *Phys. Rev. B* **92**, 155307 (2015).
 - ³² Kardar, M. Replica Bethe ansatz studies of two-dimensional interfaces with quenched random impurities. *Nucl. Phys. B* **290**, 582-602 (1987).

³³ Bornemann, F. On the numerical evaluation of Fredholm determinants. *Math. Comp.* **79**, 871-915 (2010).

³⁴ Alves, S. G., Oliveira, T. J. and Ferreira, S. C. Non-universal parameters, corrections and universality

in Kardar-Parisi-Zhang growth. *J. Stat. Mech.* P05007 (2013).

SUPPLEMENTAL TEXT

A. Summation over eigenstates of the equivalent bosonic problem and the two-time JPDF

Here we give the explicit expression of the joint moments in terms of eigenstates of the Lieb-Liniger Hamiltonian $H_{LL}^{(n)}$

$$H_{LL}^{(n)} = - \sum_{j=1}^n \partial_{x_j}^2 - 2 \sum_{i<j}^n \delta(x_i - x_j) - \frac{n}{12} \quad (1)$$

and we discuss the final steps leading to our result for the JPDF. After inserting two complete sets of eigenstates with different particle numbers, $|\mu_{n_2}\rangle$ in the first and $|\gamma_{n_1+n_2}\rangle$ in the second factor of equation (iii) in Methods, we obtain for the joint moments

$$\langle Z(0, t_1)^{n_1} Z(0, t_2)^{n_2} \rangle = \sum_{\mu_{n_2}} \sum_{\gamma_{n_1+n_2}} \langle \mu_{n_2} | \vec{0}_{n_2} \rangle \langle \vec{0}_{n_1+n_2} | \gamma_{n_1+n_2} \rangle e^{-(t_1 \Delta) E_\mu - t_1 E_\gamma} F_{\mu; \gamma}^{n_2; n_1+n_2} \quad (2)$$

where $\langle \mu_n | \vec{0}_n \rangle$ is the normalized overlap between the eigenstate $|\mu_n\rangle$ and the state $|\vec{0}_n\rangle$ where all the particles are in the same position $x = 0$. The quantities $F_{\mu; \gamma}^{n_2; n_1+n_2}$ are the so-called form factors related to the matrix elements of powers of the bosonic annihilation operator between the two eigenstates. In the Lieb-Liniger model with n particles, the eigenstates are parametrized by a set of distinct (in general complex) quasi-momenta or rapidities $\mu \equiv \{\lambda_1, \dots, \lambda_n\}$ and the eigenenergies are given by the sum $E_\mu = \sum_{\alpha=1}^n \lambda_\alpha^2 - \frac{n}{12}$. Focusing on the limit of infinite system size L , the general eigenstate is built by partitioning the n particles into a set of $n_s \leq n$ bound states called strings²⁸ formed by $m_j \geq 1$ particles with $n = \sum_{j=1}^{n_s} m_j$. Their associated rapidities are parameterized as $\lambda_{j, a_j} = k_j + \frac{i}{2}(m_j + 1 - 2a_j)$, where $m_j k_j \in \mathbb{R}$ is the total momentum of string j . Here, $a_j = 1, \dots, m_j$ labels the rapidities within the string $j = 1, \dots, n_s$. From now on a string state is denoted as $|\mu\rangle = |\mathbf{k}, \mathbf{m}\rangle$ and labeled by the set of $(k_j, m_j)_{j=1, \dots, n_s}$. Its associated eigenenergy is thus $E(\mathbf{k}, \mathbf{m}) \equiv \sum_{j=1}^{n_s} m_j k_j^2 - \frac{1}{12} m_j^3$, which is the sum of a kinetic and binding energy.

In the infinite system size limit, the coupled sum over quasi-momenta $\sum_{\{k_j\}_{j=1}^{n_s}}$ can be replaced by a product of integrals, a property also used in^{18,19,21,22}

$$\sum_{\mu_n} |\mu_n\rangle \langle \mu_n| \xrightarrow{L \rightarrow \infty} \sum_{n_s=1}^n \frac{1}{n_s!} \left(\prod_{j=1}^{n_s} \sum_{m_j=1}^n \int_{-\infty}^{+\infty} \frac{dk_j m_j}{2\pi} L \right) |\mathbf{k}, \mathbf{m}\rangle \langle \mathbf{k}, \mathbf{m}| \delta_{\sum_{j=1}^{n_s} m_j, n} \quad (3)$$

where the combinatorial factor $\frac{1}{n_s!}$ avoids double counting of states. Using that $\langle \mathbf{k}, \mathbf{m} | \vec{0}_n \rangle = L^{-n_s} \Phi[\mathbf{k}, \mathbf{m}] \prod_{j=1}^{n_s} m_j^{-2}$ where $\Phi[\mathbf{k}, \mathbf{m}] = \prod_{1 \leq i < j \leq n_s} \frac{4(k_i - k_j)^2 + (m_i - m_j)^2}{4(k_i - k_j)^2 + (m_i + m_j)^2}$ ^{18,19} we can rewrite the sum in (2) as

$$\begin{aligned} \langle Z(0, t_1)^{n_1} Z(0, t_2)^{n_2} \rangle &= \sum_{n_s^\mu=1}^{n_2} \sum_{n_s^\gamma=1}^{n_1+n_2} \frac{1}{n_s^\mu! n_s^\gamma!} \prod_{j=1}^{n_s^\mu} \left(\sum_{m_j^\mu=1}^{\infty} \int \frac{dp_j}{2\pi m_j^\mu} \right) \prod_{j=1}^{n_s^\gamma} \left(\sum_{m_j^\gamma=1}^{\infty} \int \frac{dq_j}{2\pi m_j^\gamma} \right) F_{\mathbf{p}, \mathbf{m}^\mu; \mathbf{q}, \mathbf{m}^\gamma}^{n_2; n_1+n_2} \\ &\times \delta_{n_2, \sum_{j=1}^{n_s^\mu} m_j} \delta_{n_1+n_2, \sum_{j=1}^{n_s^\gamma} m_j} \Phi[\mathbf{p}, \mathbf{m}^\mu] \Phi[\mathbf{q}, \mathbf{m}^\gamma] e^{-(t_1 \Delta) E(\mathbf{p}, \mathbf{m}^\mu) - t_1 E(\mathbf{q}, \mathbf{m}^\gamma)} \end{aligned} \quad (4)$$

where the superscripts μ and γ indicate which set of string eigenstate is considered. Since the general case is out of reach at present, in this work we restrict to the case where the state $|\gamma_{n_1+n_2}\rangle$ is constituted only by one single string of size $m = n_1 + n_2$ and momentum q (the case $q = 0$ corresponds to the ground state of the Hamiltonian (1), where all the particles form a single bound state with zero momentum). The validity of this approximation is discussed in Section B. In this case $n_s^\gamma = 1$ and the form factors can be expressed as

$$F_{\mathbf{p}, \mathbf{m}; q, n_1+n_2}^{n_2; n_1+n_2} = n_2! (n_1 + n_2)! (n_1)_{n_2} \prod_{j=1}^{n_s} \frac{1}{(0^+ + i(q - p_j) + \frac{n_1+n_2-m_j}{2})_{m_j} (0^+ - i(q - p_j) + \frac{n_1+n_2-m_j}{2})_{m_j}} \quad (5)$$

where 0^+ is a regulator that is set to zero in the final stages of the calculation and $(n)_m$ are the Pochhammer symbols. It turns out that the sum in Eq. (4), when restricted to the case $n_s^\gamma = 1$, i.e. over the remaining string lengths m_j^μ

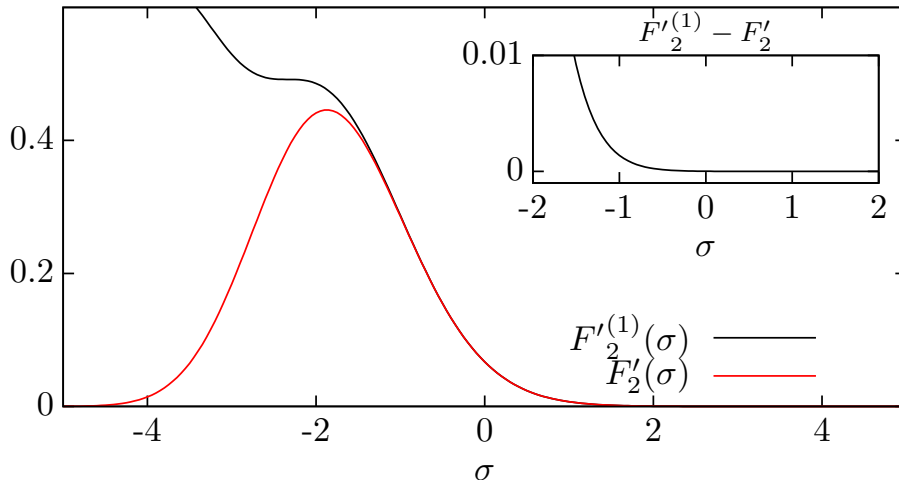


FIG. S1: Plot of the Tracy-Widom distribution $F'_2(\sigma) \equiv \partial_\sigma F_2(\sigma)$ (red line) (with $F_2(\sigma) = \det[1 - \Pi_\sigma K_{\text{Ai}}]$) compared with its tail for positive σ given by $F'^{(1)}_2(\sigma)$ (black line). Inset: difference between the Tracy-Widom distribution $F'_2(\sigma)$ and its tail $F'^{(1)}_2(\sigma)$, given in (7).

and moments p_j , can be explicitly performed for arbitrary t_1 , using extensions of methods introduced in [18,19,21,22](#). Taking the limit $t_1 \rightarrow +\infty$, we obtain the generating function $g_\Delta^{(1)}(\sigma_1, \sigma)$ discussed in the Methods. This leads to the final result for the two-time JPDF (Equation 4 in the text) in the limit $t_1 \rightarrow \infty$.

Finally we would like to point out that in Ref. [26](#) the sum over states has been implicitly restricted as $n_s^\gamma \geq n_s^\mu$. Hence important terms, not vanishing in the large time limit, have been neglected.

B. Tail approximation

In this section we discuss the validity of our approximation. The exact JPDF satisfies the sum rule

$$\int_{-\infty}^{+\infty} d\sigma P_\Delta(\sigma_1, \sigma) = F_2(\sigma_1) \quad (6)$$

where $F_2(\sigma) = \text{Det}[I - \Pi_\sigma K_{\text{Ai}}]$ is the Tracy Widom cumulative distribution function associated to the GUE ensemble, which can be expressed as a Fredholm determinant. On the other hand, our approximated result for the JPDF satisfies

$$\int_{-\infty}^{+\infty} d\sigma P_\Delta^{(1)}(\sigma_1, \sigma) = F_2^{(1)}(\sigma_1) := 1 - \text{Tr}[\Pi_\sigma K_{\text{Ai}}] = 1 - \int_\sigma^{+\infty} dv K_{\text{Ai}}(v, v) \quad (7)$$

where we have defined the "tail approximation" $F_2^{(1)}(\sigma)$ of the Tracy-Widom cumulative distribution. It corresponds to keeping only the first term in the series expansion for a determinant of a matrix near the identity $\text{Det}[I + A] = 1 + \text{Tr}A + \mathcal{O}(A^2)$. This function captures the leading (stretched) exponential behaviour for large and positive σ , $F_2^{(1)}(\sigma) - 1 = \mathcal{O}(e^{-\frac{4}{3}\sigma^{3/2}})$ and the corrections are of higher (stretched) exponential order $F_2(\sigma) = F_2^{(1)}(\sigma) + \mathcal{O}(e^{-\frac{8}{3}\sigma^{3/2}})$. In fact, one can see in Figure [S1](#) that this approximation remains excellent in a much broader range (with error less than 10^{-3} for any $\sigma > -1$). Hence, due to the sum rule (7) we expect the same to be valid also for the accuracy of our approximation $P_\Delta^{(1)}(\sigma_1, \sigma)$ of the JPDF as a function of σ_1 . Indeed, the experimental and numerical data for the conditional mean and variance are found to agree as well at $\sigma_{1c} = -1.5$ (Fig. [S3](#)).

C. Two-time rescaled conditional covariance and its large Δ limit

The two-time rescaled conditional covariance, defined in the text in equation (3), is calculated over the realizations such that $\tilde{h}_{t_1} > \sigma_{1c}$. Using our formula for the JPDF and performing an expansion at large Δ we obtain that the

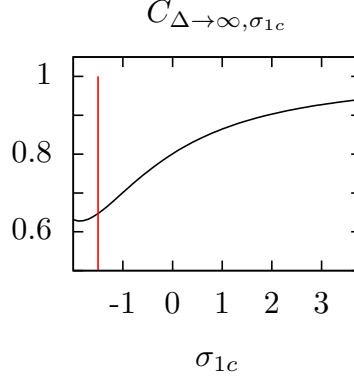


FIG. S2: Two-time rescaled conditional covariance in the infinite Δ limit, defined in (8), plotted as a function of σ_{1c} . The formula (8) is expected to give an excellent approximation for all $\sigma_{1c} \gtrsim -1.5$ (red vertical line), and deviate from the exact result for smaller values. The curve approaches 1 in the limit $\sigma_{1c} \rightarrow +\infty$. The minimum occurs at finite $\sigma_{1c} \approx -2$, while the true minimum (with value C) is expected at $\sigma_{1c} = -\infty$. The value at the minimum suggests that $C \approx 0.6$, consistent with the observations in the text (see Fig. 4 in the main text).

above covariance reaches a finite limit, given explicitly as

$$C_{\Delta \rightarrow \infty, \sigma_{1c}} := \lim_{\Delta \rightarrow +\infty, \sigma_{1c}} C_{\Delta, \sigma_{1c}} = 1 + \frac{\int_{\sigma_{1c}}^{+\infty} d\sigma_1 \sigma_1 \tilde{R}_{1/3}(\sigma_1) - \mathcal{N}_{\sigma_{1c}}^{-1} \int_{\sigma_{1c}}^{+\infty} d\sigma_1 \sigma_1 F_2^{(1)'}(\sigma_1) \int_{\sigma_{1c}}^{+\infty} d\sigma_1 \tilde{R}_{1/3}(\sigma_1)}{\int_{\sigma_{1c}}^{+\infty} d\sigma_1 \sigma_1^2 F_2^{(1)'}(\sigma_1) - \mathcal{N}_{\sigma_{1c}}^{-1} \left(\int_{\sigma_{1c}}^{+\infty} d\sigma_1 \sigma_1 F_2^{(1)'}(\sigma_1) \right)^2} \quad (8)$$

where $\mathcal{N}_{\sigma_{1c}} = 1 - F_2^{(1)}(\sigma_{1c}) = \int_{\sigma_1}^{\infty} dy K_{\text{Ai}}(y, y)$ and where $\tilde{R}_{1/3}(\sigma_1) = \left[\int_{\sigma_1}^{\infty} dy \text{Ai}(y) \right]^2 - \int_{\sigma_1}^{\infty} dy K_{\text{Ai}}(y, y)$. The function $C_{\Delta \rightarrow \infty, \sigma_{1c}}$ is plotted as a function of σ_{1c} in Fig. S2. It approaches 1 with corrections of order $\sim \sigma_{1c}^{-1}$ for large and positive σ_{1c} . For $\sigma_{1c} < -1.5$ the tail approximation becomes unreliable (see Fig. S1), and the minimum shown in the figure occurs at finite σ_{1c} , while the true minimum is expected at $\sigma_{1c} = -\infty$. Nevertheless it suggests a rough estimate for the value of $C = \lim_{\sigma_{1c} \rightarrow -\infty} C_{\Delta \rightarrow \infty, \sigma_{1c}}$ as $C_{\Delta \rightarrow \infty} \approx 0.6$.

SUPPORTING FIGURES

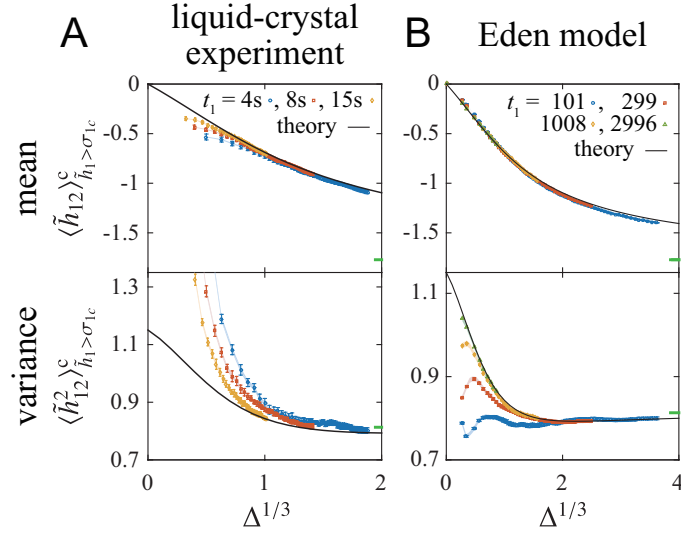


FIG. S3: Conditional mean $\langle \tilde{h}_{12} \rangle_{\tilde{h}_1 > \sigma_{1c}}^c$ and variance $\langle \tilde{h}_{12}^2 \rangle_{\tilde{h}_1 > \sigma_{1c}}^c$ with $\sigma_{1c} = -1.5$. Experimental (A) and numerical (B) data with different t_1 are shown in different colors and symbols. The regions of overlapped data indicate the asymptotic Δ -dependence, which is found to be in excellent agreement with the theoretical predictions (black lines), without any fitting parameter. The error bars indicate the standard errors, and the shaded areas show the uncertainty due to the estimation error in v_∞ and Γ . To reduce the effect of finite-time corrections, here we used such realizations that satisfy $\tilde{h}_1 > \tilde{h}_{1c}$ with $\text{Prob}[\tilde{h}_1 \geq \tilde{h}_{1c}] = 1 - F_2(\sigma_{1c})$. The deviation of the non-overlapped data is due to finite-time corrections, which decay as t_1^{-1} (Fig. S4). Note that the asymptotic theoretical curves converge to the Baik-Rains values (mean 0, variance 1.1504) at $\Delta \rightarrow 0$ and to the GUE Tracy-Widom values (mean -1.7711, variance -0.8132, indicated in the figures by the green bars) at $\Delta \rightarrow \infty$.

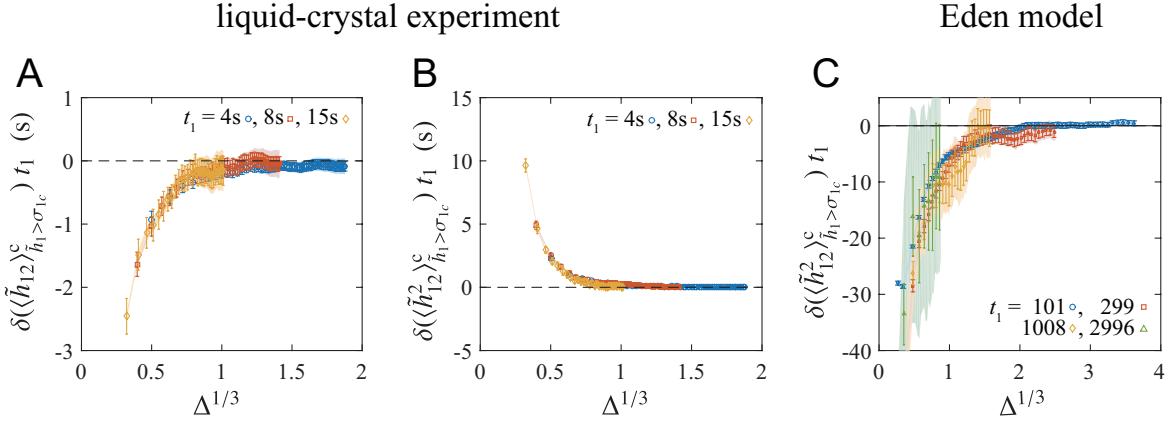


FIG. S4: Finite-time corrections in the conditional mean $\langle \tilde{h}_{12} \rangle_{\tilde{h}_1 > \sigma_{1c}}^c$ and variance $\langle \tilde{h}_{12}^2 \rangle_{\tilde{h}_1 > \sigma_{1c}}^c$. Using the experimental (a,b) and numerical (c) data for $\sigma_{1c} = -1$ and different t_1 , shown in Fig. 2 in the text, we plot the difference from the theoretically predicted values, $\delta(\langle \tilde{h}_{12} \rangle_{\tilde{h}_1 > \sigma_{1c}}^c)$, multiplied by t_1 . Overlapping of the data indicates that the finite-time corrections decay as $\delta(\langle \tilde{h}_{12} \rangle_{\tilde{h}_1 > \sigma_{1c}}^c) \sim t_1^{-1}$. The error bars indicate the standard errors, and the shaded areas show the uncertainty due to the estimation error in v_∞ and Γ . We do not show the finite-time corrections in the conditional mean for the Eden-model simulation, which were too small to evaluate their t_1 -dependence in a reliable manner.